Transient fuel performance analysis of UO₂-BeO fuel with composite SiC coated with Cr cladding based on multiphysics method

Chunyu Yin[1,2], Shixin Gao[1,2], Shengyu Liu[3],

Rong Liu[3*], Guanghui Su[1], Libo Qian[2]

1. School of Nuclear Science and Technology, Xi'an Jiaotong University, Xi'an, 710049,

China

2. Science and Technology on Reactor System Design Technology Laboratory, Nuclear Power

Institute of China, Chengdu, 610213，China

3. School of Electric Power, South China University of Technology, Guangzhou, Guangdong,

510640，China

*Corresponding author Tel: +86 2087114487;

E-mail: rliu290147@hotmail.com

1

ABSTRACT

The transient multiphysics models were updated in CAMPUS to evaluate the accident-tolerant fuel performance under accident conditions. CAMPUS is a fuel-performance code developed based on COMSOL. The simulated results of the UO_2-Zircaloy fuel performance under accident conditions were compared with those of the FRAPTRAN code and the experimental data to verify the correctness of the updated CAMPUS. Subsequently, multiphysics models of the UO_2-BeO fuel and composite SiC coated with Cr (SiC_f/SiC-Cr) cladding were implemented in CAMPUS. Finally, the fuel performance of the three types of fuel-cladding systems under Loss Of Coolant Accident (LOCA) and Reactivity Insertion Accident (RIA) condtions were evaluated and compared, including the temperature distribution, stress distribution, pressure evolution, and cladding failure time. The results showed that the fuel temperature of the UO_2 fuel under accident conditions without pre-irradiation was lower after being combined with SiC_f/SiC-Cr cladding. Moreover, the centerline and outer surface temperatures of the UO_2-BeO fuel combined with SiC_f/SiC-Cr cladding reduced further under accident conditions. The cladding temperature increased after the combination with the SiC_f/SiC-Cr cladding under accident conditions with pre-irradiation. In addition, the use of SiC_f/SiC-Cr cladding significantly reduced the cladding hoop strain and plenum pressure.

Key words: Accident condition; Fuel performance; UO_2-BeO fuel; SiC_f/SiC-Cr cladding.

1 INTRODUCTION

Since the Fukushima nuclear accident in 2011, efforts have been undertaken to evaluate accident-tolerant fuel performances. Numerical analysis is an effective and economical method to study the fuel performance. Applying this method, basic data can be provided to guide nuclear reactor design. To precisely predict the fuel performance, many computer codes/programs have been developed recently. Herein, fuel behavior models have been developed based on experimental data. The FAST code is used to analyze the fuel performance in CANDU reactors. It was developed based on the COMSOL platform by Prudil [1] at the Royal Military College. The FAST code was validated in their work. Additionally, the CANDU reactor fuel performance was analyzed under normal operating conditions. FRAPCON and FRAPTRAN are commercial licensed codes developed by Geelhood and Luscher [2]. These are used to investigate the fuel performance under normal operating and accident conditions, respectively. Thermodynamics, heat transfer, burnup, mechanics, and neutron calculations are considered in the FRAPCON and FRAPTRAN codes. Then, a new code called CAMPUS, developed based on COMSOL by Liu et al. [3], was used to investigate the fuel performance in pressurized water reactors (PWRs). The combination of

3

thorium-based fuel with two-layered SiC claddings was studied using CAMPUS under normal operating conditions [4]. Furthermore, thorium-based fuel combined with SiC_f/SiC-Cr cladding was studied using CAMPUS under both normal operation and accident conditions. The results demonstrated that the combination of thorium-based fuel with Cr-coated SiC fuel cladding can effectively improve the safety margin of fuel rods under accident conditions. Subsequently, Liao et al. [5] improved the steady-state fuel rod performance analysis code FROBA-ROD to predict the fuel rod behavior under the condition of a reactivity-initiated accident (RIA). FROBA-ROD was verified by comparing it with FALCON simulation data under RIA conditions. Moreover, codes were developed for various fuel structures. Yang et al. [6] developed a new program called DUO-THERM to analyze the heat flux and fuel temperature of an annular fuel rod. They determined that the heat flux of an annular fuel is significantly affected by the variations in the inner and outer gaps. The VVER-1200 reactor was investigated using the COMSOL platform to study the fuel performance under normal operating conditions [7]. This is important for the analyzing the fuel performance under off-normal operating conditions. In addition to the fuel behavior analysis of conventional light water reactors (LWRs), other types of reactors such as small reactors and molten salt reactors have been studied [8, 9]. The design in terms of the neutronic aspect has been researched by developing

a code named SDIC1.0, to achieve an optimized lightweight shielding design for small reactors [8]. Compared with the RMC code, the calculation time was shortened by 6.3 times. The CORE3D code was developed to investigate the coupled performance. It contains neutronic, thermohydraulic, and molten salt loop system of a molten salt reactor [9]. The results provided certain essential indications for more improved design optimization and safety analysis.

Currently, a considerable number of codes/programs have been developed to analyze the fuel behavior. However, to evaluate fuel performance more accurately, the material property models of fuel and cladding are also being developed continuously. SiC is reported to have high-temperature strength, creep resistance, low thermal expansion, and good radiation resistance [10]. It is considered to be a good substitute for Zircaloy cladding. Therefore, substantial research has been conducted on the SiC material. CVD-SiC and SiC/SiC composites are recommended to be applied as fuel rod cladding in PWRs [11]. The two-layered cladding consisting of an internal fiber-reinforced SiC/SiC composite layer and external integral CVD SiC layer substantially reduces the likelihood of cladding failure under steady state conditions [12]. Meanwhile, the MOOSE/BISON multi-physical fuel performance analysis tool was developed by Wagih et al. [13] to study the fuel performance of multi-layered zirconium/silicon carbide cladding under steady-state and

transient accident conditions in PWRs. However, after being irradiated, the thermal conductivity of SiC decreases dramatically. Therefore, it is necessary to apply a cladding material with a high thermal conductivity to mitigate or even eliminate the increase in fuel temperature caused by the use of SiC cladding. Furthermore, the performance of SiC composite cladding was studied in our previous work [14, 15]. Therein, the models of swelling, thermal conductivity, creep, etc., were implemented based on certain assumptions to analysis the behavior of SiC cladding [14]. The result indicated that the gap closure can be delayed and the stress status released using SiC cladding [15]. The failure probability of SiC cladding was evaluated by Deng et al. [16] using the Monte Carlo method. The research revealed a marginal likelihood of failure when two-layer SiC cladding is used. Meanwhile, the UO_2-BeO composite fuel is reported as one of the alternative potential accident-tolerant fuels for PWRs [17]. This is because the thermal conductivity of UO_2 fuel can be improved by mixing a small amount of BeO [18]. The common additives to the UO_2 matrix including Cr_2O_3, Al_2O_3, and TiO_2 were reported to be the most effective means to achieve long-term heat preservation [19]. Chandramouli [20] updated the UO_2-BeO attribute models in the FRAPTRAN code. He determined that the use of UO_2-BeO fuel pellets could reduce the fuel temperature under accident conditions. Kim et al. [21] from Korea Atomic Energy Research Institute performed a cost–

6

benefit analysis of the UO_2-BeO fuel. The advantages of this fuel are maximized when the BeO content is 4.8%. However, the likelihood of cladding corrosion increases as the fuel burnup increases. Therefore, the SiC_f/SiC-Cr cladding is proposed to be combined with the UO_2-BeO fuel under accident conditions. This is because the Cr coating displays good corrosion and oxidation resistance, whereas its oxidation process accelerates above 1200 °C [22]. A neutronics analysis of the UO_2-BeO fuel was conducted by Zhang et al. [23]. The research result revealed that the fuel temperature coefficient remained nearly constant notwithstanding a variation in the fraction of BeO in the UO_2-BeO. The crud of the cladding surface and coating has been widely considered to have a certain impact on the heat transfer in the fuel rod. Efforts have been undertaken to reduce the amount of crud on the cladding surface by injecting zinc in the coolant [24, 25].

Therefore, in this study, the relevant physics models for the simulations under accident conditions were updated based on CAMPUS [3]. It has been applied to analyze the fuel performance of different types of fuel rods under different operating conditions [4, 26]. The feasibility of the updated code used in this study was investigated further. The remainder of this paper is organized as follows: First, the thermodynamic properties and related physical models of UO_2-BeO fuel and SiC_f/SiC-Cr cladding are introduced. Subsequently, based on the fuel performance code

CAMPUS, transient multiphysics models are introduced to more precisely evaluate the fuel performance under accident conditions. The multiphysics models of the UO$_2$-BeO fuel and SiC$_f$/SiC-Cr cladding were implemented in CAMPUS, and the fuel performance under LOCA and RIA conditions was compared with the simulated results of FRAPTRAN to verify the updated code. Finally, the performances of the two fuel cladding combinations were investigated and compared with that of the UO$_2$-Zircaloy system under LOCA and RIA conditions.

2 MATERIAL PROPERTIES

2.1 UO$_2$-BeO fuel

As a likely candidate for ATF materials, the UO$_2$-BeO fuel has a high melting point, low neutron absorption, low thermal expansion coefficient, and good chemical compatibility. Moreover, BeO is suitable for increasing the thermal conductivity because its thermal conductivity is significantly higher than that of the UO$_2$ fuel [27]. In this section, the properties of the UO$_2$-BeO fuel are introduced.

2.1.1 Thermal conductivity

The thermal conductivity of UO$_2$-BeO was calculated using the following formula recommended by Chandramouli et al. [20]:

$$k = k_{UO_2-BeO} \times FD \times FP \times FM \times FR \tag{1}$$

$$k_{UO_2-BeO} = k_{95,UO_2-BeO} \times \left(\frac{1}{1-(2.6-0.5 \times T_n) \times 0.05} \right) \tag{2}$$

8

$$k_{95,UO_2-BeO} = \frac{1}{0.0375 + 0.0002165T - 0.034248 - 0.000315VT} + \frac{4.75 \times 10^9}{T^2} \exp\left(-\frac{16361}{T}\right)$$

(3)

$$FP = 1 + \left(\frac{0.019\beta_p}{3.0 - 0.019\beta_p}\right)\left(\frac{1.0}{1.0 + \exp\left(\frac{-(T-1200)}{100}\right)}\right)$$

(4)

$$FD = \left(\frac{1.09}{\beta_p^{3.265}} + 0.0643\sqrt{\frac{T}{\beta_p}}\right) \cdot \arctan\left(\frac{1.0}{\frac{1.09}{\beta_p^{3.265}} + 0.0643\sqrt{\frac{T}{\beta_p}}}\right)$$

(5)

$$FM = \left(\frac{1.0 - p}{1.0 + (\sigma_s - 1)p}\right)$$

(6)

$$FR = 1 - \frac{0.2}{1.0 + \exp\left(\frac{T-900}{80}\right)}$$

(7)

where k_{95,UO_2-BeO} is the thermal conductivity of the unirradiated and fully dense UO$_2$-BeO fuel; FD, FP, FM, and FR are factors for the dissolved fission products, precipitated fission products, Maxwell porosity effect, and radiation effect, respectively; β_p is the burnup of the UO$_2$-BeO fuel; σ_s is the shape factor (1.5 for spherical pores); and p is the porosity.

2.1.2 Thermal capacity

The thermal capacity of the UO$_2$-BeO fuel was calculated using a mass-weighted interpolation calculation as follows [20]:

$$C_{p,UO_2-BeO} = W_{UO_2} \times C_{p,UO_2} + W_{BeO} \times C_{p,BeO}$$

(8)

$$C_{p,BeO} = 1000 \times \left(0.036 \times \left(\frac{T-650}{360}\right)^3 - 0.12 \times \left(\frac{T-650}{360}\right)^2 + 0.2 \times \left(\frac{T-650}{360} + 1.9\right)\right)($$

9)

9

$$W_{BeO} = \frac{V_{BeO} \times \rho_{BeO}}{V_{UO_2} \times \rho_{UO_2} + V_{BeO} \times \rho_{BeO}} \quad (10)$$

where W_{UO_2} and W_{BeO} are the weight fractions of UO_2 and BeO, respectively; T is the temperature in K; V_{UO_2} and V_{BeO} are the volume fractions of UO_2 and BeO, respectively; and ρ_{UO_2} and ρ_{BeO} are the densities of UO_2 and BeO, respectively.

According to Carbajo's [28] recommendation, the heat capacity of UO_2 was calculated using the MATPRO-11 correlation:

$$C_p(UO_2) = \frac{296.7\theta^2 \exp\left(\frac{\theta}{T}\right)}{T^2\left(\exp\left(\frac{\theta}{T}\right)-1\right)} + 0.0243T + \frac{8.75 \times 10^7 YE_D}{2RT} \times \exp\left(\frac{-E_D}{RT}\right) \quad (11)$$

where T is the temperature in K, Y is the oxygen-to-metal ratio, R is the universal gas constant = 8.315 J/mol/K, θ is the Einstein temperature for UO_2 and is set to 535.285 K, and E_D is the activation energy for Frenkel defects and is set to 1.577×10^5 J/mol for UO_2 fuel.

2.1.3 Density and thermal expansion

The density and thermal expansion of the UO_2-BeO fuel were calculated by interpolation based on the volume fraction:

$$\rho_{UO_2-BeO} = \upsilon_{UO_2} \times \rho_{UO_2} + \upsilon_{BeO} \times \rho_{BeO} \quad (12)$$

where ρ_{UO_2} is as recommended by Fink [29]:

$$\rho_{UO_2} = 10970 \times \left(a + bT + cT^2 + dT^3\right)^{-3} \quad (13)$$

The parameters in Eq. (13) are listed in Table 1:

Table 1 Parameter of formula (13)

Temperature	a	B	c	d
T≤923K	0.99734	9.802×10^{-6}	-2.705×10^{-10}	4.391×10^{-13}
T>923K	0.99672	-1.179×10^{-5}	-2.429×10^{-9}	-1.2195×10^{-12}

The BeO fuel density was introduced by Liu et al. [18]. The formula is as follows:

$$\rho\left(BeO\right)=0.21\times\left(\left(T-1200\right)/530\right)^{4}+2.6\times\left(\left(T-1200\right)/530\right)^{3} \\ -3\times\left(\left(T-1200\right)/530\right)^{2}-63\times\left(\left(T-1200\right)/530\right)+2900 \tag{14}$$

where T is the temperature in K.

The thermal expansion of UO_2-BeO fuel was calculated by the following equation:

$$\left(\frac{\Delta L}{L}\right)_{UO_2-BeO}=V_{UO_2}\times\left(\frac{\Delta L}{L}\right)_{UO_2}+V_{BeO}\times\left(\frac{\Delta L}{L}\right)_{BeO} \tag{15}$$

where ρ is the density of the fuel and $\frac{\Delta L}{L}$ is its thermal expansion.

2.1.4 Young's modulus and Poisson's ratio

The volume fraction was used to calculate the Young's modulus and Poisson's ratio of the fuel:

$$E_{UO_2-BeO}=V_{UO_2}\times E_{UO_2}+V_{BeO}+E_{BeO} \tag{16}$$

$$E_{BeO}=3.5\times10^{11}Pa \tag{17}$$

$$\upsilon_{BeO}=0.229 \tag{18}$$

where V is the volume fraction of the material, E is the Young's modulus of the fuel, and υ is the Poisson's ratio.

2.2 SiC material properties

The related material properties of SiC implemented in CAMPUS are

summarized in this section.

2.2.1 Thermal conductivity

The thermal conductivity of the SiC composite was calculated by the thermal resistance model proposed by Snead et al. and Stone et al. [30, 31]. The relevant formula is as follows:

$$k_{SiC-CMC} = \frac{1}{R_0 + R_{irr}} \quad (19)$$

$$R_0 = \frac{1}{k_{SiC}} \quad (20)$$

$$k_{SiC} = -1.71 \times 10^{-11} T^4 + 7.35 \times 10^{-8} T^3 - 1.10 \times 10^{-4} T^2 + 0.061T + 7.97 \quad (21)$$

$$R_{irr} = 6.08 \times S \quad (22)$$

$$S = S_s \times \left[1 - \exp\left(1 - \frac{\gamma}{\gamma_c} \right) \right]^{\frac{2}{3}} \quad (23)$$

$$S_s = 5.8366 \times 10^2 - 1.0089 \times 10^{-4} T - 6.9368 \times 10^{-8} T^2 - 1.8152 \times 10^{-11} T^3 \quad (24)$$

$$\gamma_c = -0.57533 + 3.3342 \times 10^{-3} T - 5.3970 \times 10^{-6} T^2 + 2.9754 \times 10^{-9} T^3 \quad (25)$$

where R_0 is the thermal resistance of the SiC composite cladding without irradiation, S is the irradiation expansion strain, γ is the displacement per atom (DPA) of SiC, S_s is the saturation expansion rate, and T is the cladding temperature.

2.2.2 Heat capacity

The following model proposed by Snead et al. [30] was adopted to calculate the heat capacity of the SiC composite cladding:

$$C_p = 925.65 + 0.377T - 7.926 \times 10^{-5} T^3 - \frac{3.195 \times 10^7}{T^2} \quad (26)$$

2.2.3 Young's modulus

The Young's modulus of the SiC composite material was calculated using the following equation. The unirradiated Young's modulus was calculated using the value 230 GPa measured by Koyanagi and Katoh [32]. The influence of irradiation on Young's modulus was calculated according to the formula recommended by Mieloszyk [33].

$$E_{SiC,non-irr} = 230 \ GPa \tag{27}$$

$$E_{irr} = E \times \left(1 - 0.15\left(\frac{\Delta V}{V}\right)\right) \tag{28}$$

2.2.4 Poisson's ratio

The Poisson's ratio of the SiC composite material was also based on Mieloszyk's [33] work. A fixed value of 0.13 was adopted:

$$\upsilon_{SiC} = 0.13 \tag{29}$$

2.2.5 Thermal expansion

According to Katoh et al. [34], the thermal expansion coefficient of the SiC composite cladding is calculated as follows:

$$\alpha(T) = 10^{-6}\left(-0.7765 + 1.435\times10^{-2}T - 1.2209\times10^{-5}T^2 + 3.8289\times10^{-9}T^3\right) \tag{30}$$

where $\alpha(T)$ denotes the thermal expansion coefficient in 1/K, the reference temperature is 293 K, and T denotes the cladding temperature in K.

2.3 Material properties of pure Cr

The material properties of pure Cr used in the Cr-coated Zircaloy cladding models are summarized below.

2.3.1 Thermal conductivity

According to Holzwarthand et al. [35], the thermal conductivity of pure Cr between 300 K and 1300 K can be calculated using the following formula:

$$\lambda(T) = \left(-2.07 \times 10^{-8} T^3 + 4.85 \times 10^{-5} T^2 - 0.06T + 101.75\right) \quad (31)$$

where T is the temperature in K and $\lambda(T)$ is the thermal conductivity in W/m/K.

2.3.2 Heat capacity

The heat capacity was calculated as follows [35]:

$$C_p(T) = \left(-1.28 \times 10^{-7} T^3 + 3.39 \times 10^{-4} T^2 - 0.09T + 483.2\right) \quad (32)$$

where T is the temperature in K and $C_p(T)$ is the heat capacity in J/mol/K.

2.3.3 Young modulus

The Young's modulus of pure Cr was calculated according to the method proposed by Armstrong [36] as follows:

$$E(T) = -2.50 \times 10^{-5} T^2 - 0.01T + 264.11 \quad (33)$$

where T is the temperature in K and $E(T)$ is Young's modulus in GPa.

2.3.4 Thermal expansion coefficient

The formula recommended by Holzwarthand et al. [35] was used to calculate the thermal expansion coefficient of pure Cr.

$$\alpha(T) = \left(1.27 \times 10^{-10} T^3 + 5.41 \times 10^{-7} T^2 + 0.0015T + 7.87\right) \times 10^{-6} \quad (34)$$

where T is the Cr temperature with a reference temperature of 293 K.

14

2.3.5 Thermal creep rate

The Norton creep law was used to calculate the thermal creep rate of Cr according to Stephens and Klopp [37]:

$$\dot{\varepsilon} = 3.2555 \times 10^{-40} \times \exp\left(-\frac{306268.8}{8.3145T}\right)\sigma^{6.2} \tag{35}$$

2.3.6 Poisson's ratio

The Poisson's ratio can be approximated as a constant [38]:

$$\upsilon = 0.22 \tag{36}$$

3 MULTIPHYSICS MODEL DEVELOPMENT AND VERIFICATION

The specific modeling geometry and computational mesh in this study are shown in Figure 1(a). These are consistent with those in our previous work [3]. The two-dimensional axisymmetric geometry and SiC_f/SiC-Cr cladding were adopted in this work. Ten fuel-rod pellet lengths were simulated by setting periodic boundary conditions along the axial direction of a fuel pellet. An information flowchart of the multi-physics models is shown in Figure 1(b).

(a)

（b）
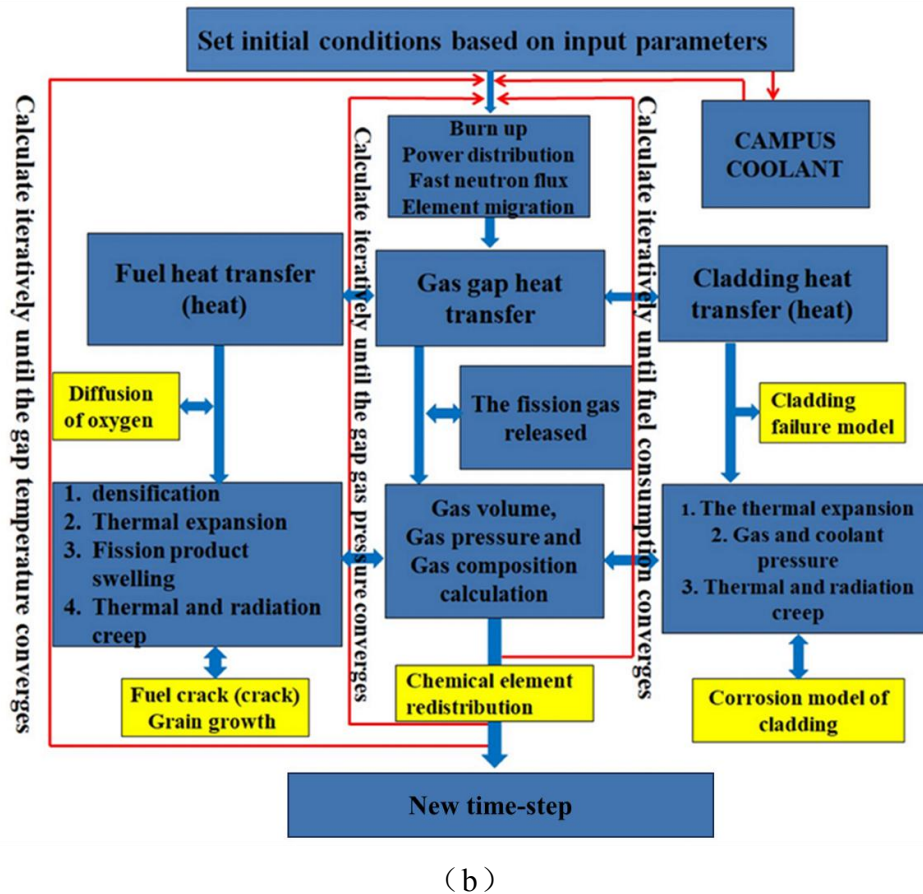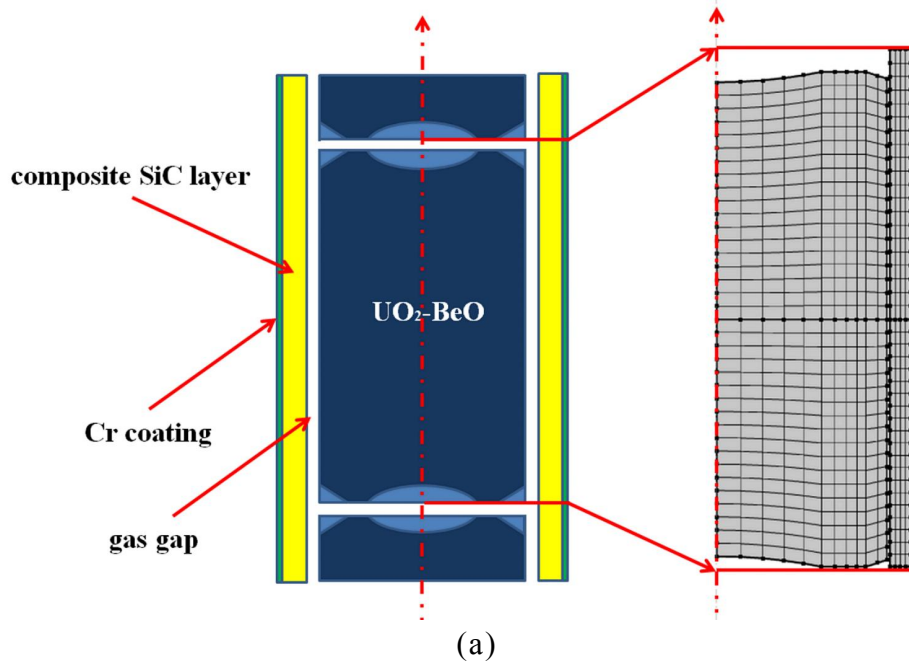
Figure 1(a) Modeling geometry and computational mesh of UO$_2$-BeO fuel

with the SiC$_f$/SiC-Cr cladding; (b) Information flowchart of multiphysics

models

**3.1 Physics models under accident condition**

3.1.1 Coolant model

Based on the COMSOL platform, a simplified coolant model was developed to simulate the coolant loss and provide an approximate evaluation of the heat flux on the outer surface of the cladding. In this model, the coolant is divided into water and steam states based on the input parameters of the subchannel radius and cooling water mass flow. Subsequently, 13 points are set on the fuel rods to extract the corresponding data for the axial position of the cladding outer surface temperature under LOCA conditions.

To verify the correctness of this model, the variations in the outer surface temperature of the cladding under the accident condition (LOCA MT-1) were simulated and compared with the simulated results of the FRAPTRAN code. This is depicted in Figure 2(a) and 2(b). As shown in Figure 2(b), the temperature difference between nodes 7 and 9 was caused by the difference in coolant conditions between these two codes. In CAMPUS, a simplified coolant condition was adopted that divided the coolant into two states (liquid and vapor). Therefore, the temperature of a certain point on the outside of the cladding increased continuously when the corresponding coolant state was vapor and decreased dramatically when the corresponding coolant state was liquid. This was different from the coolant conditions set in the FRAPTRAN code. However, the overall

temperature trends of these two codes were similar. Therefore, the analysis and conclusions were not affected by this factor.
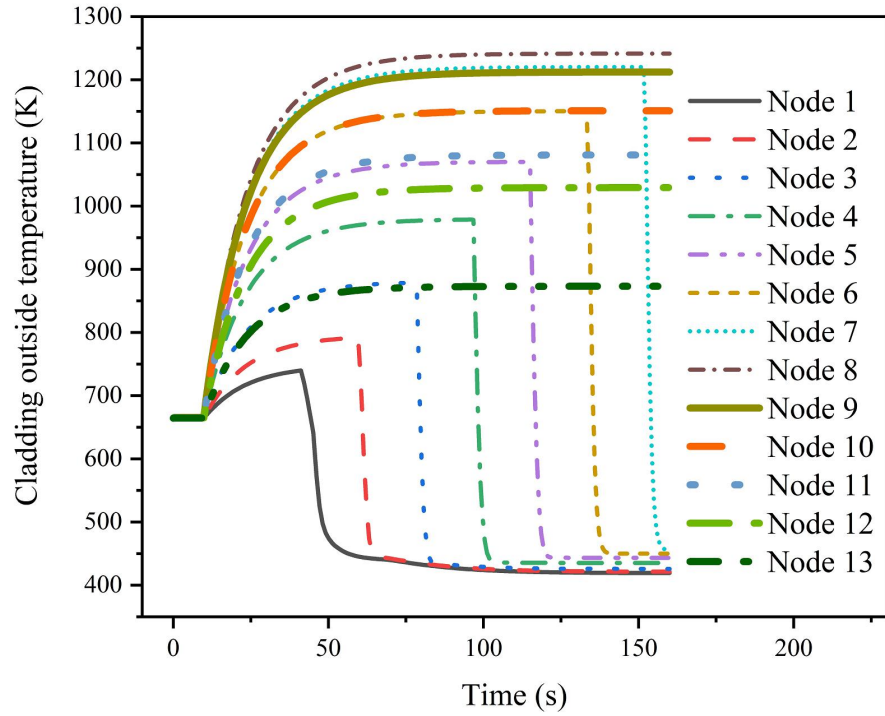
(a)
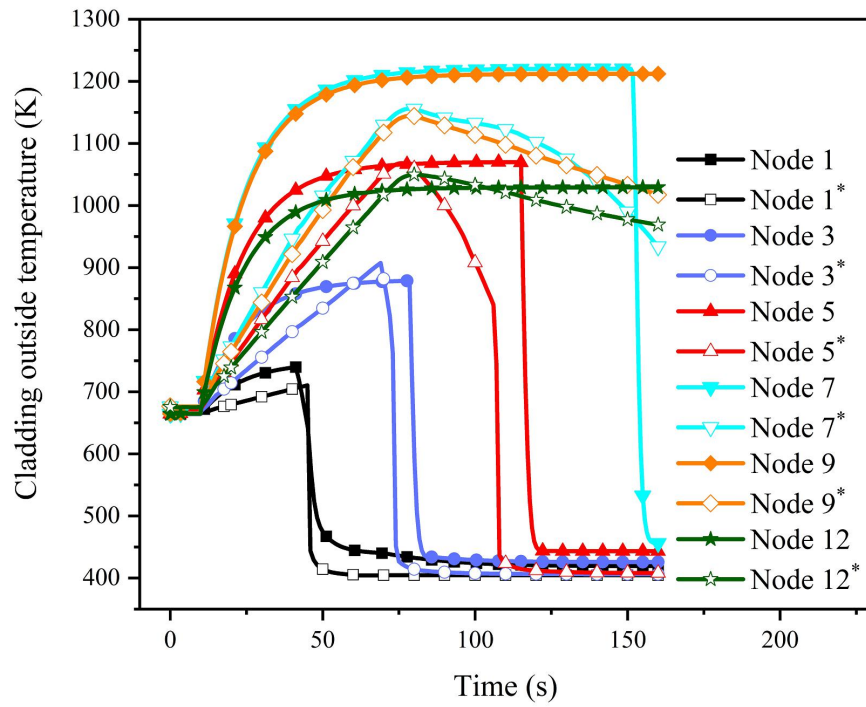
(b)

Figure 2(a) CAMPUS-calculated results of cladding outer temperature

under LOCA condition; (b) Comparison of cladding node temperature

simulation results of CAMPUS and FRAPTRAN under LOCA condition

(the node with the symbol * is the simulation results of FRAPTRAN)

3.1.2 High-temperature creep model

Under accident conditions, a large creep deformation and thermal expansion of the cladding were observed in high-temperature conditions. For the accident analysis, a strain-rate model was adopted to simulate the large creep deformation of the cladding [39].

$$\dot{\varepsilon}_{eff} = A \times \exp\left(-\frac{Q}{RT}\right) \times \sigma_{eff}^n \tag{37}$$

where $\dot{\varepsilon}_{eff}$ is the effective cladding creep rate in 1/s, A is the strength coefficient in $MPa^{-n}s^{-1}$, Q is the creep activation energy in J/mol, σ_{eff} is the cladding effective stress in MPa, and n is the stress exponent. The parameters adopted (summarized in Table 2) were obtained by tensile tests on a Zircaloy cladding [40]. In the mixed phase ($\alpha + \beta$) region, the Norton parameters were interpolated between the parameters of the pure α and pure β phases. These are summarized in Table 2 [40]:

Table 2 Parameters of creep model

Phase state	$\dot{\varepsilon}_{eff}(s^{-1})$	A（$MPa^{-n}s^{-1}$）	Q(J/mol)	n
α	Any	8737	$3.21 \times 10^{10}+$ $24.69 \times (T-923.15)$	5.89
50%α 50%β	$\leq 3 \times 10^{-3}$	0.24	102366	2.33
	$>3 \times 10^{-3}$	ln(A) linear interpolation	Linear interpolation	linear interpolation

| β | any | 7.9 | 141919 | 3.78 |

The creep in the SiC composite layer was evaluated using the creep model proposed by Snead [30].

$$\dot{\varepsilon} = 2 \times 10^3 \times \left(\frac{\sigma}{191 \times 10^3}\right)^{2.3} \times \exp\left(-\frac{174000}{8.314T}\right) + 2.7 \times 10^{-35} \sigma\phi \qquad (38)$$

where σ denotes the effective stress in MPa, ϕ denotes the neutron flux in n/m^2, and T denotes the temperature in K.

3.1.3 Cladding failure model

The ultimate strain model in FRAPTRAN [41] was used to predict the cladding failure:

$$\begin{aligned}\varepsilon_{fail} &= 1.587979 \times 10^{-9} T^4 - 6.92798 \times 10^{-6} T^3 + 1.053049 \times 10^{-2} T^2 \\ &\quad - 7.331051T + 1906.22 \qquad\qquad \left(940\ K < T < 1200\ K\right)\end{aligned} \qquad (39)$$

$$\begin{aligned}\varepsilon_{fail} &= -1.67939 \times 10^{-8} T^3 + 6.23050 \times 10^{-5} T^2 - 7.360497 \times 10^{-2} \\ &\quad + 28.1199 \qquad\qquad \left(1200\ K < T < 1700\ K\right)\end{aligned} \qquad (40)$$

$$\varepsilon_{fail} = 0.544589 \qquad\qquad \left(T > 1700\ K\right) \qquad (41)$$

where ε_{fail} is the ultimate strain of the Zircaloy cladding (m/m) and T is the cladding temperature (K). As recommended by Lamon et al. [42], when the hoop strain of an SiC$_f$/SiC-Cr cladding exceeds 0.6%, the cladding fails.

3.1.4 Swelling and fission gas release model

The models recommended by Liu et al. [18] were used to simulate the swelling and fission gas release processes.

3.2 Code verification under LOCA accident

The flexibility and accuracy of CAMPUS have been demonstrated

and verified [43]. To further verify the correctness of CAMPUS under accident condition, in this work, the LOCA MT-4 case reported in the Pacific Northwest Laboratory (PNL) LOCA simulation program was selected for the model verification. The experiment funded by the U.S. Nuclear Regulatory Commission (NRC) aims to evaluate fuel behavior under LOCA conditions in the temperature range of 1033–1200 K (1400– 1700 °F) [44]. The experimental parameters are listed in Table 3. The LOCA condition was simulated primarily by setting the boundary condition of the heat transfer coefficient on the cladding outer surface. A simplified coolant model was adopted to calculate the heat-transfer coefficient of the cladding outer surface under LOCA conditions.

Table 3 Parameters of MT-4 case

Parameter	Value
Fuel pellet height (mm)	11.90
Fuel pellet radius (mm)	4.1
Cladding inner radius (mm)	8.36
Cladding outer radius (mm)	9.5
Ratio of cavity height to fuel rod height	0.045
Fuel concentration	5%
Initial fuel density	95% theoretical
Linear power density (kW/m)	1.24
Coolant pressure (MPa)	0.28

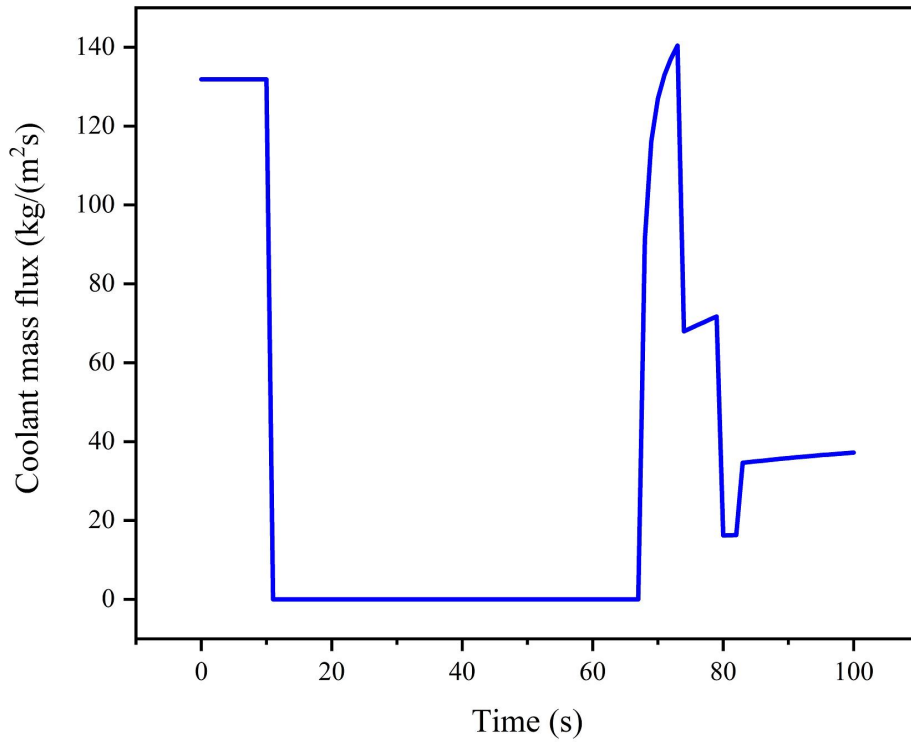|	
Coolant water (K)	530
Initial burnup (MWd/kgU)	40
Initial pressure (MPa)	9.3

Figure 3 Coolant mass flux data for MT-4 case

The variation in the coolant mass flow rate evolution for the MT-4 case is shown in Figure 3. The relevant parameters were implemented in the CAMPUS coolant model to set appropriate boundary conditions at the outer surface of the cladding. As shown in Figures 2 and 3, the heat transfer process of the outer surface of the cladding was calculated correctly under the LOCA condition using the coolant model introduced in this study.

The simulated results of the updated CAMPUS were compared with

those of the FRAPTRAN code and the measured data from the MT-4 experimental report to verify the correctness of the updated CAMPUS. The comparisons are shown in Figure 4(a) and 4(b).
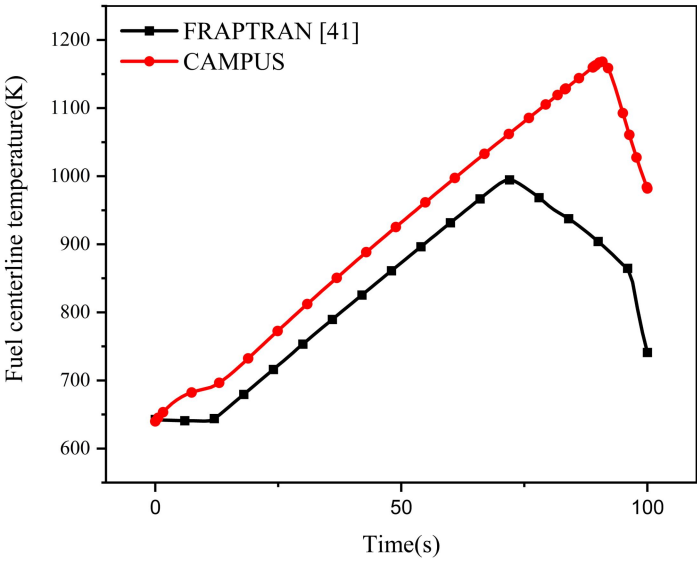
(a)
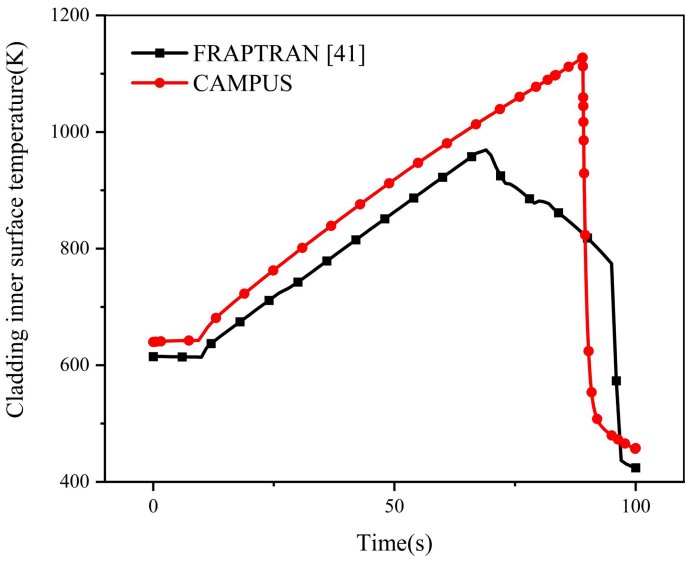
(b)

Figure 4 (a) Fuel centerline temperature comparisons of FRAPTRAN and CAMPUS under LOCA condition; (b) Cladding inner surface temperature comparisons of FRAPTRAN and CAMPUS under LOCA condition

As presented in Figure 4(a) and 4(b), the fuel central temperature increased gradually under LOCA condition (10 s), the heating process continued until the reflooding process occurred, and the fuel temperature decreased rapidly because of the reflooding process. The updated CAMPUS displayed a temperature variation consistent with that of FRAPTRAN.

As shown in Figure 4(b), the decrease in the cladding temperature simulated by the updated CAMPUS was observed to occur after that of FRAPTRAN because the reflooding process was considered in the updated CAMPUS. As the phase of the coolant water (water and steam) changed, the heat transfer coefficient varied, and the temperature of the corresponding part of the cladding reduced dramatically. The cladding temperature started to decrease as reflooding began. This was also consistent with the results calculated using FRAPTRAN.
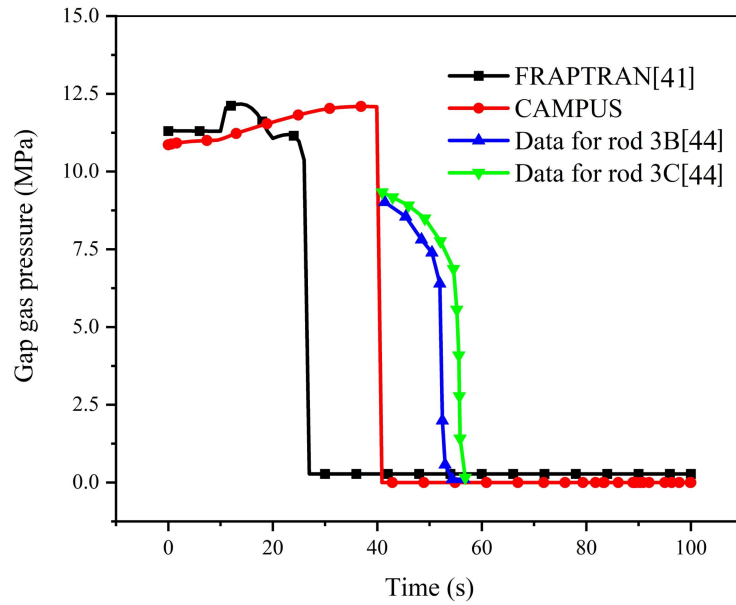
Figure 5 The experimentally measured results [44] and calculated results
of fuel rod internal gap gas pressure simulated by updated CAMPUS and

FRAPTRAN codes under LOCA condition

Figure 5 shows the experimental data and calculated gas pressure. The gas pressure in the fuel gap increased gradually with respect to the temperature under LOCA conditions. After cladding failure, the gas pressure was set equal to the external coolant pressure owing to leakage of the internal gas. The updated CAMPUS accurately predicted the variation in plenum pressure under LOCA conditions, because the calculated results were closer to the experimental results than those simulated by the FRAPTRAN code. In addition, based on the simulated cladding failure times listed in Table 4, the updated CAMPUS predicted the cladding failure time more accurately.

Table 4 Predicted results of cladding failure time

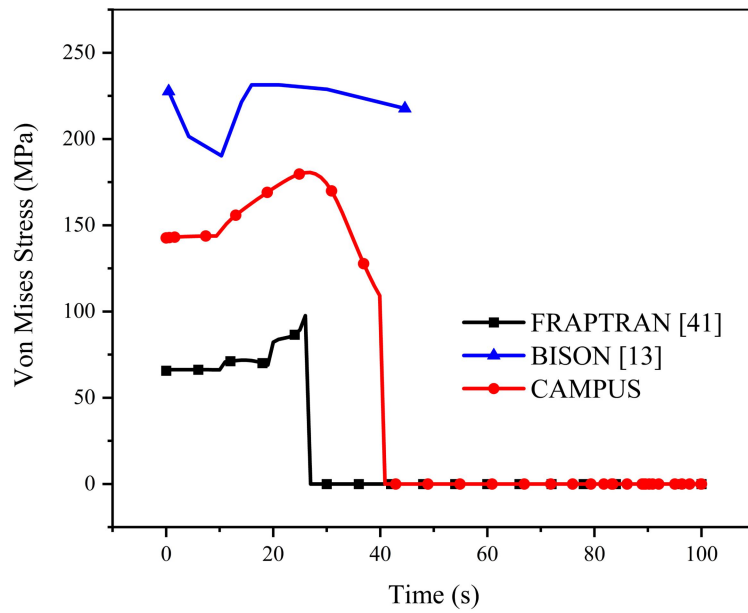| Data sources	Updated CAMPUS	FRAPTRAN	Experiment [44]
LOCA case	39.897 (s)	27 (s)	52-58 (s)
RIA case	Not failed	Not failed	Not failed

Figure 6 Von Mises stress evolutions calculated by three codes under

LOCA condition

Figure 6 compares the Von Mises stress calculated by the three codes. Because of the deficiency of stress-related experimental data for MT-4, the simulated results calculated by the FRAPTRAN and BISON codes were selected for comparison. It should be noted that in the case simulated by BISON, a Cr layer was coated on the Zircaloy cladding. However, according to Malik, Cr-coated Zircaloy claddings and Zircaloy claddings

are reported to have nearly identical thermal and mechanical properties [13]. Therefore, the result for the MT-4 case calculated by BISON where the Cr-coated Zircaloy cladding was installed was adopted for comparison. As shown in Figure 6, the cladding Von Mises stress calculated by the updated CAMPUS displayed an evolution trend similar to those of the FRAPTRAN and BISON codes. Meanwhile, the value of the Von Mises stress was between those of the BISON and FRAPTRAN codes because different mechanical models are used in different codes. Therefore, the mechanical behaviors of the fuel and cladding simulated by the updated CAMPUS under LOCA conditions had a certain degree of feasibility and accuracy.

3.3 Code verifications under RIA condition

The RIA-NA3 case from the CABRI tests was selected as the simulation case under the RIA condition in this work [2]. The power history during the RIA-NA3 case is shown in Figure 7, and the input parameters adopted from the FRAPTRAN input card are shown in Table 5. As shown in Figure 10, the fuel power increased to approximately 200000 kW/m within 0.02 s. This resulted in the generation of a large amount of heat by the fuel pellet. The response of the fuel temperature should be evaluated.

Table 5 Input parameters of NA3 case

Input parameters	Value

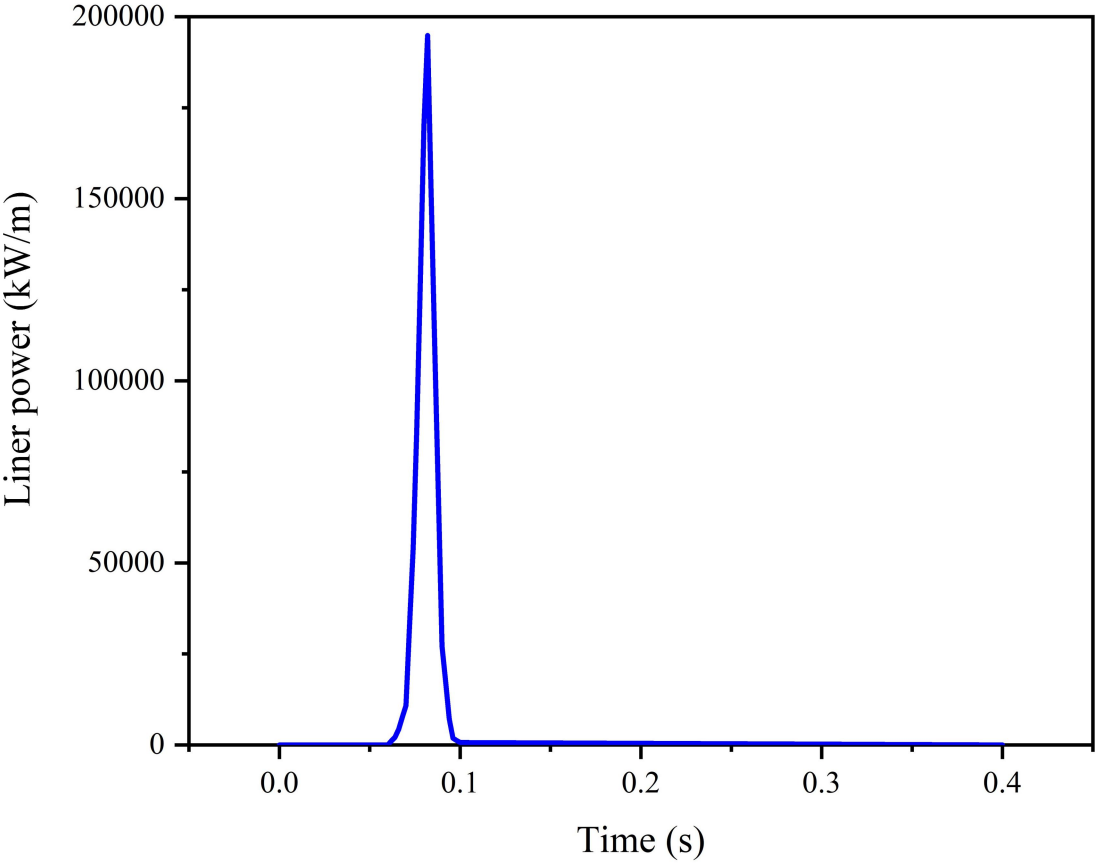|	
Fuel pellet height (mm)	11.90
Fuel pellet radius (mm)	4.1
Cladding inner radius (mm)	8.36
Cladding outer radius (mm)	9.5
Ratio of cavity height to fuel rod height	0.045
Fuel concentration	5%
Initial fuel density	95% theoretical
Linear power density (kW/m)	See in Figure 10
Coolant pressure (MPa)	0.5
Initial burnup (MWd·kgU^{-1})	51.74
Initial pressure (MPa)	0.609

Figure 7 Linear power of NA3 case
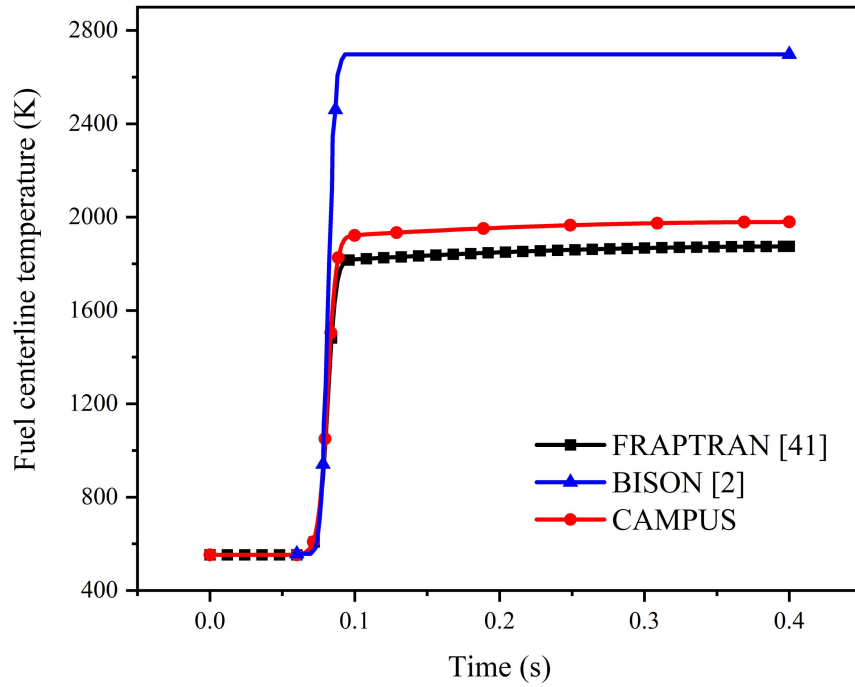
(a)
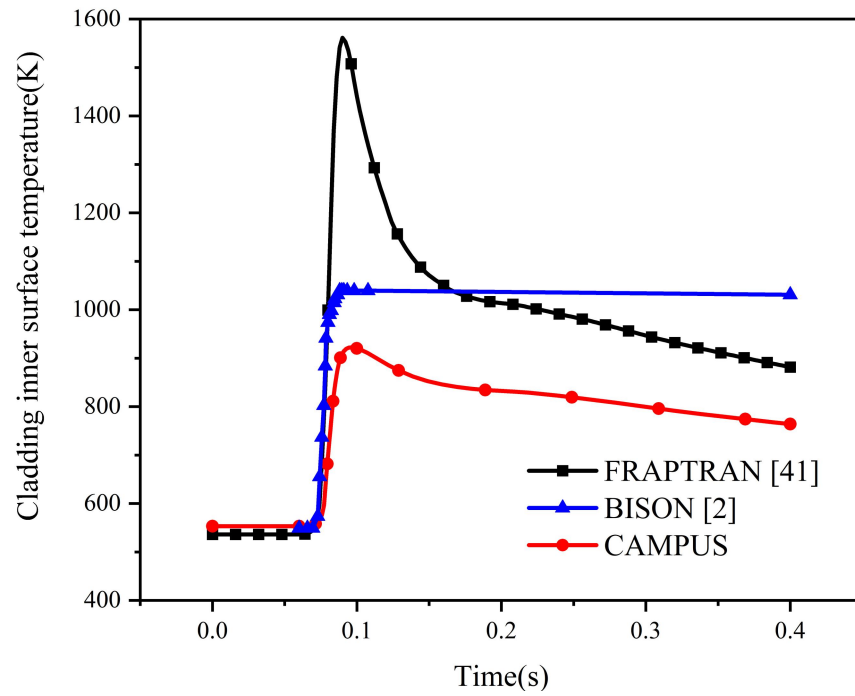
(b)

Figure 8 (a) Fuel centerline temperature evolutions calculated by the three

codes under RIA condition; (b) Cladding inner surface temperature

evolutions calculated by the three codes under RIA condition

The fuel centerline and cladding inner surface temperatures under the RIA condition simulated by the three types of codes are depicted in Figure 8(a) and 8(b), respectively. In Figure 8(a), the temperature evolutions simulated by the three codes are essentially identical. Meanwhile, the fuel centerline temperature simulated by BISON is approximately 800 K higher than those of FRAPTRAN and the updated CAMPUS.

With regard to the cladding inner surface temperature, the results calculated by FRAPTRAN show that it fluctuates significantly relative to the variation in the power. The results simulated by the updated CAMPUS have similar but more conservative cladding inner-surface temperature evolution. Nevertheless, the variations in the cladding inner surface temperature simulated by the three types of codes are relatively consistent. Therefore, the reliability and accuracy of the updated CAMPUS could be demonstrated under RIA conditions.
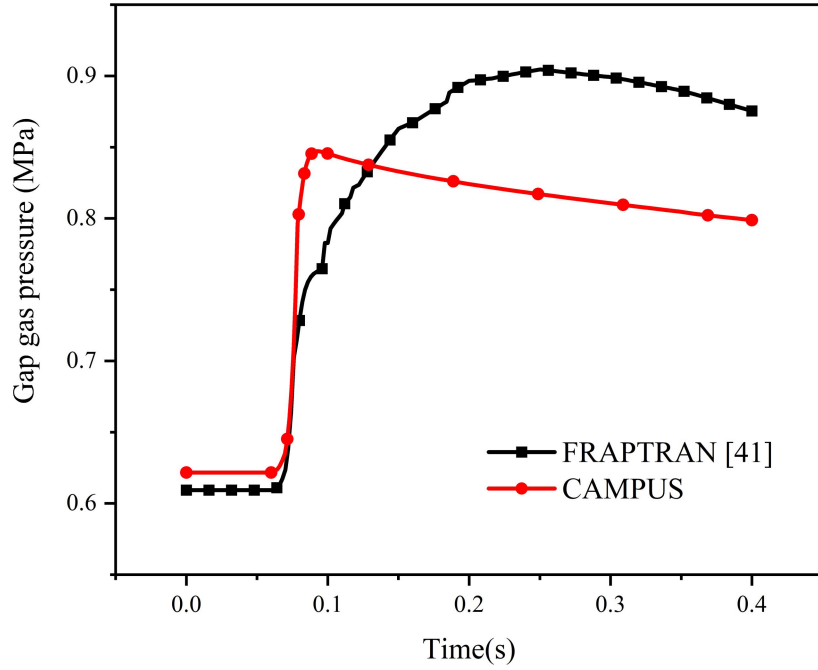
Figure 9 Gap gas pressure evolutions calculated by FRAPTRAN and

CAMPUS under RIA condition

The internal gap gas pressure under the RIA condition is depicted in Figure 9. The predicted results of the updated CAMPUS and FRAPTRAN codes for the gap gas pressure display a similar trend, although a marginal difference between the two codes is observed.
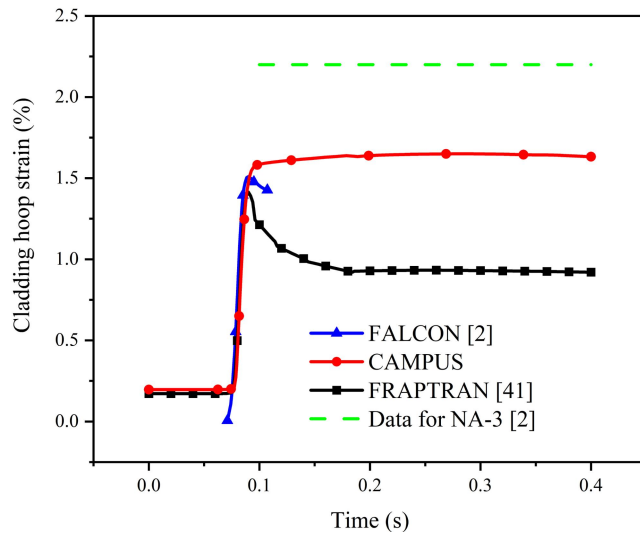

Figure 10 Cladding hoop strain experimental data and simulated results of

different codes under RIA condition

As shown in Figure 10, the evolution of the cladding hoop strain simulated using the CAMPUS, FALCON, and FRAPTRAN codes was compared with the experimental measurement data. The variation trends of hoop strains in the cladding simulated by these three codes were essentially identical, whereas the result simulated by the updated CAMPUS was closer to the experimental measurement data than those obtained by the FALCON and FRAPCON codes. This indicated that the updated CAMPUS can precisely predict the fuel performance under RIA conditions.

4 RESULTS AND DISCUSSIONS

In this study, the MT-4 case was selected to assess the fuel behavior of the three types of fuel cladding systems under LOCA conditions. First, the outer temperature of the SiC_f/SiC-Cr cladding was calculated using the CAMPUS coolant model. The corresponding heat flux was observed at selected nodes of the SiC_f/SiC-Cr cladding. The SiC_f/SiC-Cr cladding combined with UO_2-BeO fuel and UO_2 fuel was simulated using the updated CAMPUS. Then, the simulated results were compared with the UO_2-Zircaloy system. These results are analyzed and discussed in detail in the following section.

The fuel central temperature and cladding inner temperature evolutions of the three types of fuel cladding systems under LOCA conditions are compared in Figure 11(a) and 11(b), respectively. In Figure

32

11(a), a marginal decrease in the fuel central temperature is observed with the application of the SiC$_f$/SiC-Cr cladding. This is inconsistent with the reported result of an increase in the fuel central temperature as a result of the use of irradiated SiC/SiC composite cladding [8]. With the impact of the fuel central temperature shown in Figure 11(a), the cladding inner temperature of the combination of the UO$_2$-BeO fuel and SiC$_f$/SiC-Cr cladding was observed to be the lowest (see Figure 11(b)). Meanwhile, a marginal decrease in the fuel temperature was observed because the thermal conductivity for the SiC$_f$/SiC-Cr cladding was larger than that for Zircaloy cladding. As shown in Figure 11(c), the thermal conductivity of the SiC$_f$/SiC-Cr cladding decreased rapidly after irradiation. Therefore, in a pre-irradiation accident, the temperature of the fuel-cladding system equipped with the SiC$_f$/SiC-Cr cladding is likely to increase because of the abrupt decrease in the thermal conductivity of the irradiated SiC cladding. Therefore, the UO$_2$-BeO fuel combined with SiC$_f$/SiC-Cr cladding exhibited a better temperature performance than the same fuel combined with Zircaloy cladding. The overall fuel temperature reduced by approximately 100 K. This is favorable for achieving a higher fuel burnup and effectively improving the cladding stress and strain performance.

(a)

(b)

34
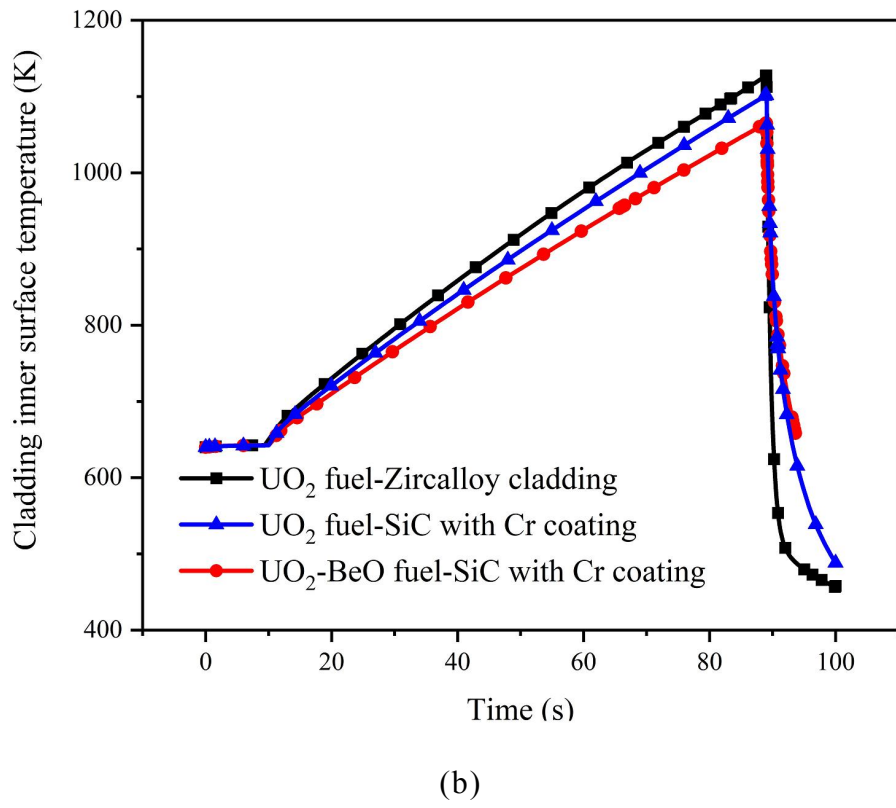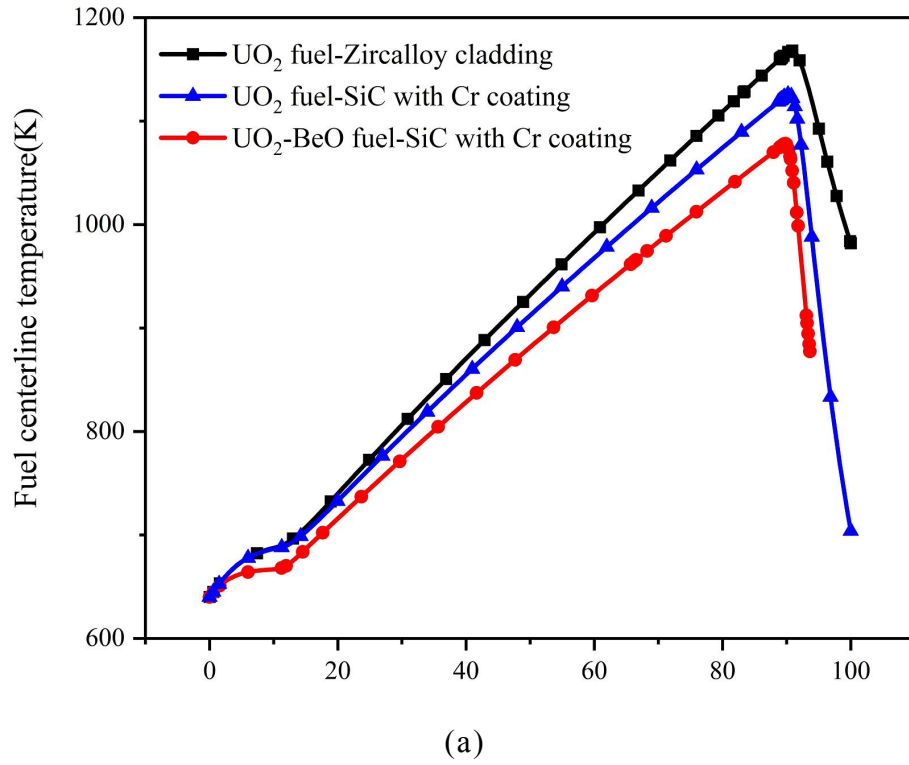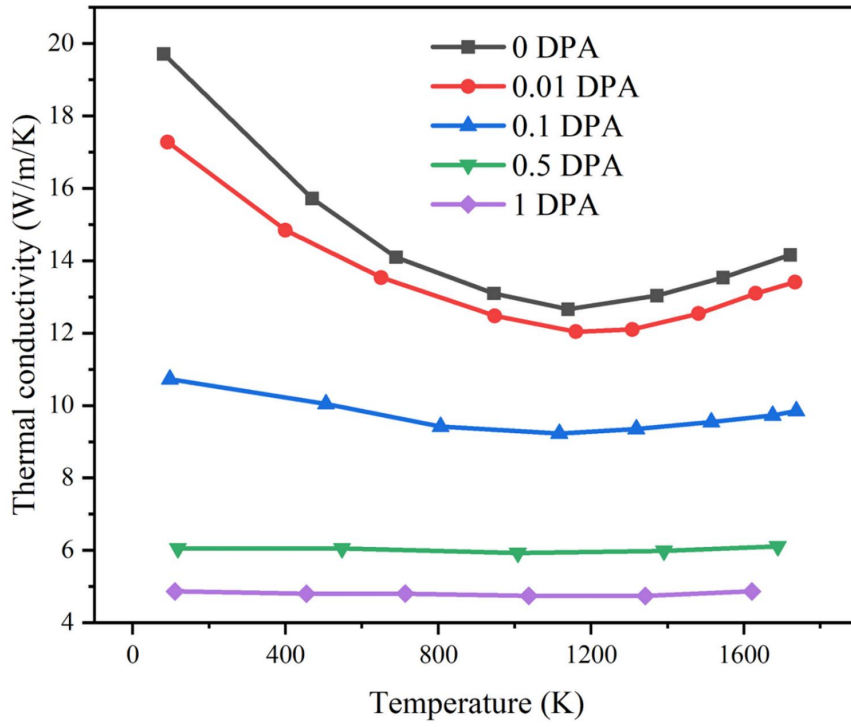
(c)

Figure 11(a) Fuel centerline temperature evolutions of three types of fuel
cladding systems under LOCA condition; (b) Cladding inner surface
temperature evolutions of three types of fuel cladding systems under
LOCA condition; (c) Thermal conductivity of SiC_f/SiC-Cr cladding under
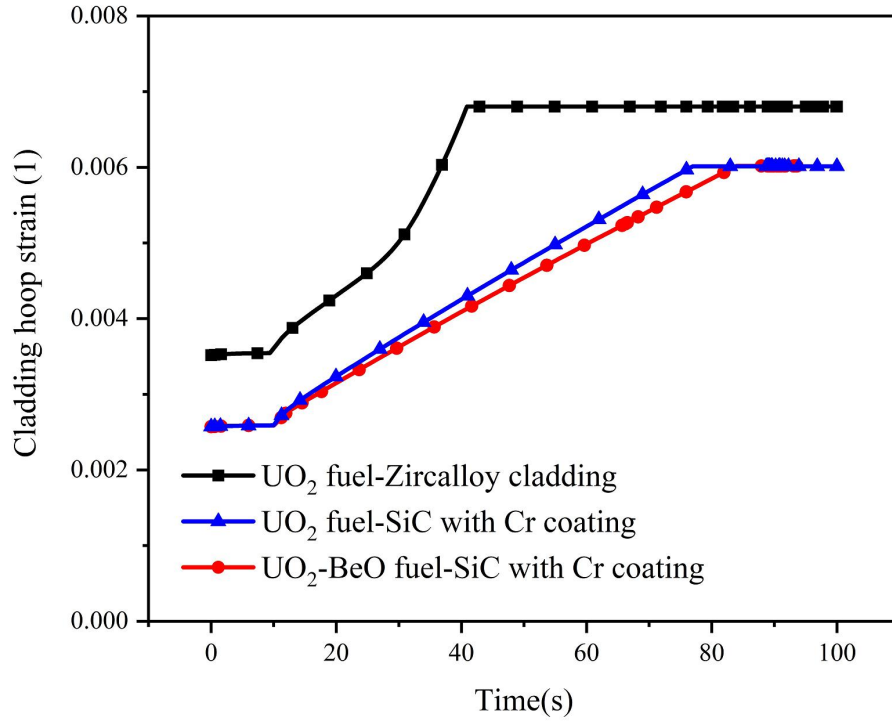different irradiation levels

Figure 12 Cladding hoop strain evolutions of three types of fuel cladding

systems

The cladding hoop strains of the three types of fuel cladding systems under LOCA conditions are shown in Figure 12. At 10 s, the hoop strain of the cladding increased immediately for the three types of fuel-cladding systems because of the increase in the cladding temperature. Furthermore, the hoop strain in the cladding increased gradually as the reflood process began. This occurred because there was a positive correlation between the hoop strain and temperature in the cladding. In addition, it can be observed from Figure 12 that the fuel-cladding system with the SiC_f/SiC-Cr cladding had a lower strain under the LOCA condition. This occurred because the use of this cladding reduced the temperature. The mechanical properties were superior to those of the Zircaloy cladding.

The safety margin is enhanced further using the UO_2-BeO fuel. This is because it has a larger thermal conductivity, which results in a uniform overall stress distribution of the fuel and cladding. Thus, the fuel performance is likely to improve, and the cladding failure time can be delayed significantly. The failure times of the three types of fuel–cladding combination systems are listed in Table 6. Compared with the Zircaloy cladding, the failure time was delayed by approximately 30 s using the SiC_f/SiC-Cr cladding. This substantially enhanced the safety of the reactor.

Table 6 Predicted failure time of three types of fuel cladding systems

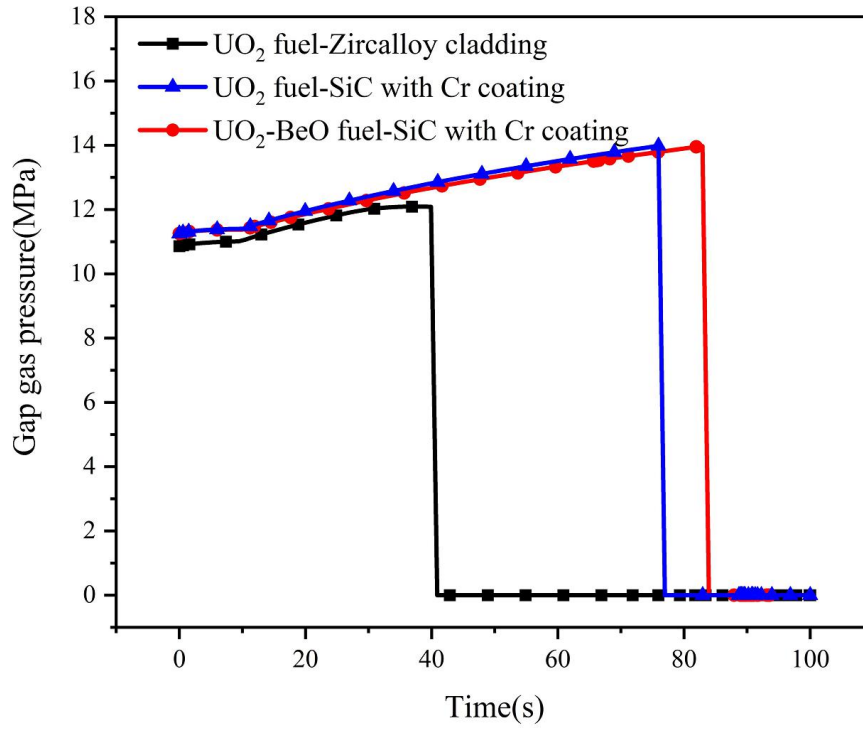| Fuel	UO_2	UO_2	UO_2-BeO
Cladding	Zircaloy cladding	SiC_f/SiC-Cr cladding	SiC_f/SiC-Cr cladding
LOCA case	39.897 s	75.968 s	81.949 s
RIA case	Not failed	Not failed	Not failed

Figure 13 Gap gas pressure evolutions of three types of fuel cladding

systems

The variation in the gap gas pressure for the three types of fuel

cladding systems under LOCA conditions is shown in Figure 13. The

evolution of the gap gas pressure for these fuel cladding systems followed

an essentially identical trend. The gap gas pressure was set equal to the

coolant pressure when the cladding failed because the internal gas leaked

rapidly. In addition, the fuel equipped with the SiC_f/SiC-Cr cladding was

simulated to fail after the same fuel equipped with the Zircaloy cladding.

This resulted in the pressure drop occurring after that of the Zircaloy

cladding. Overall, the fuel cladding system equipped with the SiC_f/SiC-Cr

cladding and UO_2-BeO fuel performed essentially similar to that with

Zircaloy in terms of gas pressure under LOCA conditions. No significant

improvement in fuel performance was observed.
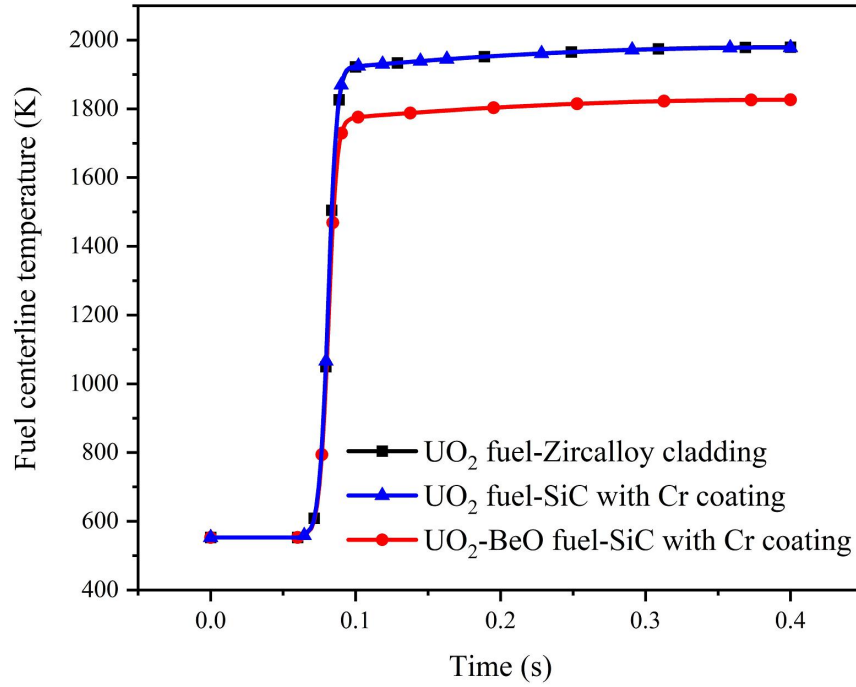
(a)
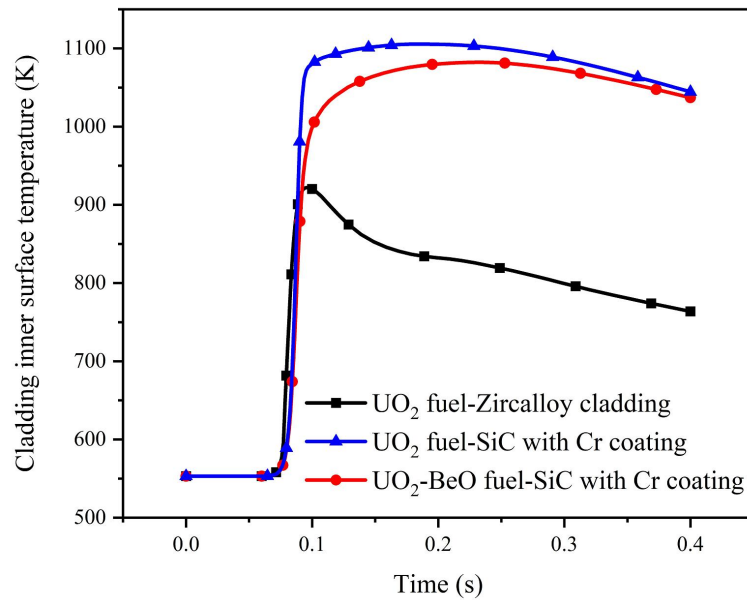
(b)

Figure 14(a) Fuel centerline temperature evolutions of three types of fuel

cladding systems; (b) Fuel inner surface temperature evolutions of three

types of fuel cladding systems

The NA3 case was selected for the simulation under the RIA condition. The fuel central temperature evolutions of the different fuel systems under the RIA condition are compared in Figure 14(a). The central temperatures of the three fuel cladding systems increased rapidly after the power pulse occurred (0.08 s). The UO_2 fuel with the Zircaloy and SiC_f/SiC-Cr claddings was observed to have an almost equal fuel central temperature. The temperature of the UO_2-BeO fuel-SiC_f/SiC-Cr cladding was approximately 200 K lower than that of UO_2 because of the higher thermal conductivity of the UO_2-BeO fuel. Nevertheless, the use of SiC_f/SiC-Cr cladding also did not have a positive impact on the temperature under the RIA conditions. Figure 14(b) shows the evolution of the cladding inner surface temperature for the three types of fuel cladding systems. The SiC_f/SiC-Cr cladding temperature was observed to be approximately 200–300 K higher than that of the Zircaloy cladding because the fuel was irradiated before the RIA condition. This resulted in a severe decrease in the thermal conductivity of the SiC_f/SiC-Cr cladding. This variation hindered the heat generated by the pellets from being transferred from the cladding to the coolant. Although the time for the RIA case was significantly short, it produced a large amount of heat within 0.2 s as the power attained a significantly high value during this period. The two factors mentioned above contributed to the difference in the cladding

temperature. However, the temperature increase of the Cr-coated cladding was reasonable. This was because this cladding did not react with the coolant and exhibited better mechanical properties.
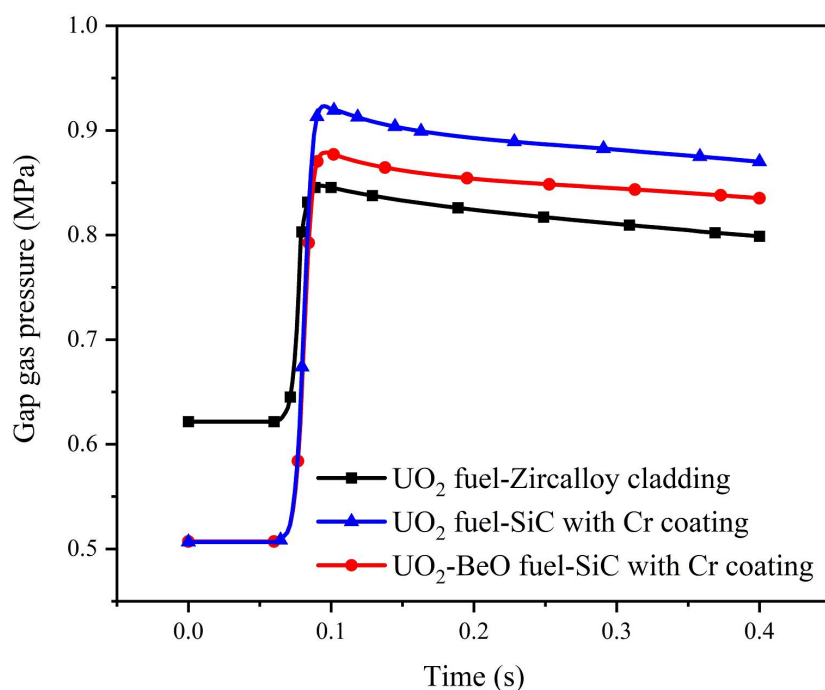
Figure 15 Gap gas pressure evolutions of three types of fuel cladding systems

As depicted in Figure 15, the gap gas pressure variations of the three types of fuel cladding systems were evaluated under the RIA conditions. The variation trends were observed to be identical. However, the gap gas pressure of the UO_2 fuel-SiC_f/SiC-Cr cladding was the lowest at the beginning and increased as the power increased. Owing to the inconsistent mechanical properties of the two types of claddings, the gap width was set to be different. This resulted in different plenum volumes and pressures. After the power pulse, the fuel-cladding system with SiC_f/SiC-Cr cladding had a higher gap gas pressure than the Zircaloy cladding based on the
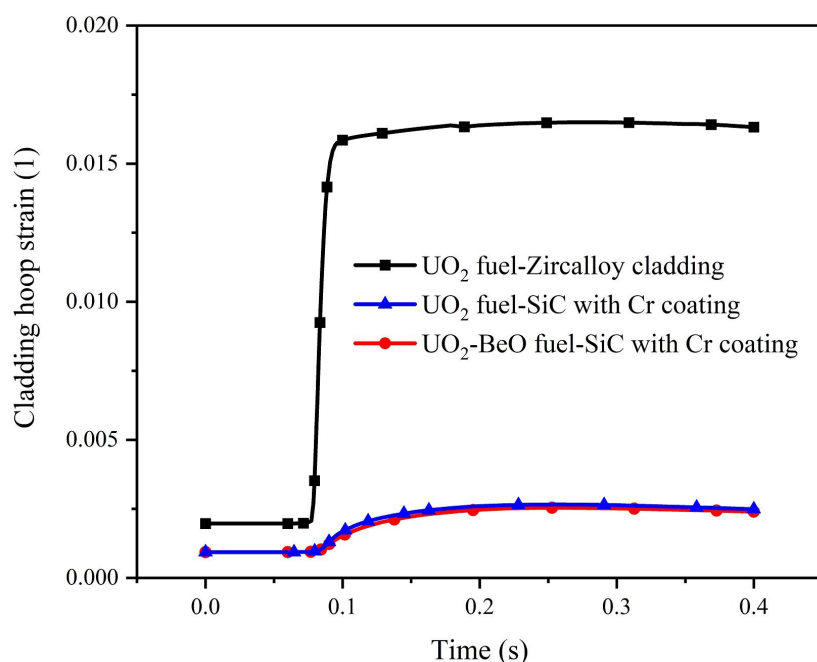
ideal gas law.

Figure 16 Cladding hoop strain evolutions of three types of fuel cladding systems under RIA condition

The hoop strains in the cladding for the three types of fuel cladding systems under the RIA conditions are compared in Figure 16. The hoop strain of the Zircaloy cladding increased significantly when the power pulse began. Moreover, the hoop strain in the cladding was reduced dramatically by applying the UO_2-BeO fuel because the temperature in the cladding was reduced effectively by applying the UO_2-BeO fuel. Thus, the SiC_f/SiC-Cr cladding was demonstrated to marginally enhance the fuel performance under the RIA conditions. Furthermore, the fuel performance was improved significantly by applying the UO_2-BeO fuel under the RIA conditions.

5 CONCLUSIONS

In this study, the simplified coolant model, fuel creep model under high-temperature conditions, bursting criterion, and other relevant thermodynamic models were implemented in CAMPUS to emulate the fuel behavior under accident conditions. The reliability of the updated CAMPUS was verified by comparing the fuel performance simulated by CAMPUS with that simulated by other codes (e.g., BISON and FRAPTRAN) and experimentally reported data under LOCA and RIA conditions. In addition, the material property models of the UO_2-BeO fuel and SiC_f/SiC-Cr cladding were collected and introduced. Finally, the fuel performance of the UO_2 fuel combined with Zircaloy cladding, UO_2 fuel with the SiC_f/SiC-Cr cladding, and UO_2-BeO fuel with the SiC_f/SiC-Cr cladding was comprehensively calculated and analyzed under both LOCA and RIA conditions. The main conclusions are summarized below:

1. Under the LOCA conditions, the SiC_f/SiC-Cr cladding improved the safety margin because it was inert to the coolant at high temperatures. Moreover, the mechanical properties of the cladding were improved significantly using the SiC_f/SiC-Cr cladding. Furthermore, no temperature increase was observed when the unirradiated SiC_f/SiC-Cr cladding was applied. This was owing to its high thermal conductivity. The cladding failure time could be delayed significantly.

2. Pre-irradiation was considered under the RIA accident conditions. Heat

43

accumulation on the inner surface of the cladding was caused by the use of the SiC_f/SiC-Cr cladding. It was difficult to conduct heat from the cladding to the coolant. This resulted in an increase in the inner surface temperature of the cladding.

3. The addition of BeO to the UO_2 fuel effectively increased the fuel thermal conductivity and thus, reduced the fuel centerline temperature and cladding outer surface temperature. Therefore, the temperature increase caused by the SiC_f/SiC-Cr cladding could be mitigated. The combination of UO_2-BeO fuel and SiC_f/SiC-Cr cladding displayed a smaller cladding hoop strain than the UO_2-Zircaloy fuel cladding systems under accident conditions.

To summarize, the UO_2-BeO composite fuel combined with SiC_f/SiC-Cr cladding can provide a better fuel performance and higher safety margin in un-irradiated LOCA conditions. Under the RIA conditions, a smaller cladding hoop strain was observed for the combination of UO_2-BeO fuels and the SiC_f/SiC-Cr cladding.

It should also be noted that the feasibility of reducing the fuel temperature by adding BeO to the fuel was a preliminary investigation. In addition, the cooling effect caused by different amounts of BeO, the trade-off between the amount of BeO and thermodynamic performance, and the neutron economy of the fuel should be evaluated further.

REFERENCES

1. A. Prudil, Andrew Albert, FAST: a Fuel and Sheath Modeling Tool for CANDU Fuel. PhD Thesis. Royal Military College of Canada, (2014).

2. K. J. Geelhood, W. G. Luscher, FRAPTRAN1.5: Integral Assessment, PNNL-19400, Vol. 2, Rev. 1. (2014). https://www.nrc.gov/docs/ML1429/ML14295A633

3. R. Liu, A. Prudil, W. Zhou et al., Multiphysics coupled modeling of light water reactor fuel performance. Prog Nucl Energy. **91** 38–48, (2016). doi.org/10.1016/j.pnucene.2016.03.030

4. R. Liu, J. Cai, W. Zhou, Multiphysics modeling of thorium-based fuel performance with a two-layer SiC cladding in a light water reactor. Ann Nucl Energy. **136**, 107036 (2020). doi.org/10.1016/j.anucene.2019.107036

5. H. Liao, K. Lu, C. Li et al., Development of a transient module based on FROBA-ROD code and assessment for fuel rod performance under reactivity-initiated accident. Ann Nucl Energy. **160**, 108377 (2021).

doi.org/10.1016/j.anucene.2021.108377

6. Y.S. Yang, C.H. Shin, T.H. Chun et al., Evaluation of a Dual-Cooled Annular Fuel Heat Split and Temperature Distribution Evaluation of a Dual-Cooled Annular Fuel Heat Split. J Nucl Sci Technol. **178**, 267 (2012). doi.org/10.1080/18811248.2007.9711593.

7. Khaled M. Yassin, Mohamed H. Hassan, Mohammad M. Ghoneim, et al. Multiphysics simulation of VVER-1200 fuel performance during normal operating conditions. Nuclear Science and Techniques **34**, 28 (2023). doi.org/10.1007/s41365-023-01172-9

8. Song-Chuan Zheng, Qing-Quan Pan, Huan-Wen Lv, et al. Semi-empirical and semi-quantitative lightweight shielding design algorithm. Nuclear Science and Techniques **34**, 43 (2023). doi.org/10.1007/ s41365-023-01187-2

9. Xian-Di Zuo, Mao-Song Cheng, Yu-Qing Dai, et al. Flow field effect of delayed neutron precursors in liquid-fueled molten salt reactors. Nuclear Science and Techniques **33**, 96 (2022). doi.org/10.1007/ s41365-022-01084-0

10. J.A. Yingling, Bison Simulation-Based Identification of Important Design Criteria for U_3Si_2 Fuels With Composite-Monolithic Duplex Sic Cladding, Scholar Commons. (2019). https://scholarcommons.sc.edu/etd

11. Y. Long, L.J. Siefken, P. Hejzlar et al., The behavior of ThO_2-based

fuel rods during normal operation and transient events in LWRs. Nucl Technol. **147**, 120–139 (2004). doi.org/10.13182/NT04-A3519

12. T. Zhang, R. Yue, X. Wang et al., Failure probability analysis and design comparison of multi-layered SiC-based fuel cladding in PWRs. Nucl Eng Des. **330**, 463–479 (2018). doi.org/10.1016/j.nucengdes.2018.02.017

13. M. Wagih, Fuel Performance of Multi-Layered Zirconium and Silicon Carbide Based Accident Tolerant Fuel Claddings, (2018). https://dspace.mit.edu/bitstream/handle/1721.1/119049/1059518711-MIT

14. C. Yin, S. Liu, Y. Jiao et al., Thermodynamic performance simulation of SiC composite cladding under transient conditions (In Chinese). Science and Technology Innovation Herald (2019). 10.16660/j.cnki.1674-098X.2019.29.101

15. C. Yin, R. Liu, Y. Jiao et al., Fuel Performance Analysis of Light Water Reactor Based on the Combination of U_3Si_2 Fuel and Two-Layer SiC Cladding Based on Multi-Physical Field Coupling (In Chinese). Nuclear Power Eng. **43**, 102–109 (2022). 10.13832/j.jnpe.2022.01.0102

16. Y. Deng, Y. Yin, Y. Wu et al., Failure Probabilistic Assessment of the Silicon Carbide Cladding Based on the Monte Carlo Method (In Chinese), Nucl Sci Eng (2021).

17. Q. Zhang, X. Wang, Y. Zhang et al., Neutronic analysis for potential Accident Tolerant Fuel UO$_2$-BeO in the light water reactor. Ann Nucl Energy. **127**, 278–292 (2019). doi.org/10.1016/j.anucene.2018.12.014

18. R. Liu, W. Zhou, P. Shen et al., Fully coupled multiphysics modeling of enhanced thermal conductivity UO$_2$-BeO fuel performance in a light water reactor. Nucl Eng Des. **295**, 511–523 (2015). doi.org/10.1016/j.nucengdes.2015.10.019

19. Y. Zhong, R. Gao, B. Li et al., Preparation and Characterization of Large Grain UO$_2$ for Accident Tolerant Fuel. Front Mater. **8**, 1–12 (2021). doi.org/10.3389/fmats.2021.651074.

20. D. Chandramouli, S.T. Revankar, Development of Thermal Models and Analysis of UO$_2$-BeO Fuel during a Loss of Coolant Accident. Int J Nucl Energy, **1–9**, 751070 (2014). doi.org/10.1155/2014/751070

21. S.K. Kim, W.I. Ko, H.D. Kim et al., Cost-benefit analysis of BeO-UO2 nuclear fuel. Prog Nucl Energy. **52**, 813–821 (2010). doi.org/10.1016/j.pnucene.2010.07.008

22. Ming Lei, Weiwei, Xiao, Jinghao. Huang. Study on high temperature oxidation behavior of Cr-coated Zr-4 alloy prepared by multi-arc ion plating (In Chinese). NUCLEAR TECHNIQUES **45**, 100202 (2022). doi.org/10.11889/j.0253-3219.2022.hjs.45.100202

23. Q. Zhang, C. Wang, X. Chi et al., Neutroic Analysis for Accident Tolerant Fuel UO$_2$-BeO in Fuel Assembly of Pressurized Water

Reactor (In Chinese). Atomic Energy Science and Technology **54**, 95 (2020). doi: 10.7538/yzk.2019.youxian.0039

24. Jiapeng, Liao, Yulong, Mao, Tianming, Ruan, et al. Effect of zinc injection on crud deposition and boron precipitation on fuel cladding surface (In Chinese). NUCLEAR TECHNIQUES **46**, 030603 (2023). doi.org/10.11889/j.0253-3219.2023.hjs.46.030603.

25. Jiapeng, Liao, Jie, Ye, Desheng, Jin, et al. Effect of core power variation on crud deposition behavior on fuel cladding surface (In Chinese). NUCLEAR TECHNIQUES **45**, 080605 (2022). doi.org/10.11889/j.0253-3219.2022.hjs.45.080605.

26. S. Liu, R. Liu, C. Qiu et al., Multiphysics modeling of thorium-based fuel performance with Cr-Coated SiC/SiC composite under normal and accident conditions. Front Energy Res. **9**, 1–14 (2021). doi.org/10.3389/fenrg.2021.677606

27. W. Zhou, W. Zhou, Enhanced thermal conductivity accident tolerant fuels for improved reactor safety – A comprehensive review. Ann Nucl Energy. **119**, 66–86 (2018). doi.org/10.1016/j.anucene.2018.04.040

28. J.J. Carbajo, G.L. Yoder, S.G. Popov et al., A review of the thermophysical properties of MOX and UO_2 fuels. J Nucl Mater. **299,** 181–198 (2001). doi.org/10.1016/S0022-3115(01)00692-4.

29. J.K. Fink, Thermophysical properties of uranium dioxide. J Nucl Mater.

279, 1–18 (2000). doi.org/10.1016/S0022-3115(99)00273-1.

30. L.L. Snead, T. Nozawa, Y. Katoh et al., Handbook of SiC properties for fuel performance modeling. J Nucl Mater. **371**, 329–377 (2007). doi.org/10.1016/j.jnucmat.2007.05.016.

31. J.G. Stone, R. Schleicher, C.P. Deck et al, Stress analysis and probabilistic assessment of multi-layer SiC-based accident tolerant nuclear fuel cladding. J Nucl Mater. **466**, 682–697 (2015). doi.org/10.1016/j.jnucmat.2015.08.001.

32. T. Koyanagi, Y. Katoh, Mechanical properties of SiC composites neutron irradiated under light water reactor relevant temperature and dose conditions. J Nucl Mater. **494**, 46–54 (2017). doi.org/10.1016/j.jnucmat.2017.07.007.

33. A.J. Mieloszyk, Assessing thermo-mechanical performance of ThO and SiC clad light water reactor fuel rods with a modular simulation tool. PhD thesis. Massachusettes Institute of Technology, Cambridge, (2015). dspace.mit.edu/handle/1721.1/103660?show=full.

34. Y. Katoh, L.L. Snead, T. Cheng et al., Radiation-tolerant joining technologies for silicon carbide ceramics and composites. J Nucl Mater. **448,** 497–511 (2014). doi.org/10.1016/j.jnucmat.2013.10.002.

35. U.Holzwarth, H. Stamm, Mechanical and thermomechanical properties of commercially pure chromium and chromium alloys. J Nucl Mater. **300**, 161–177 (2002). doi.org/10.1016/S0022-3115(01)00745-0.

36. P. E. Armstrong, Institute of Metals Division – Dynamic Young's Modulus Measurements above 1000℃ on Some Pure Polycrystalline Metals and Commercial Graphites Trans. Metall Soc. AIME. **230**, 962–966 (1964).

37. J.R. Stephens, W.D. Klopp, High-temperature creep of polycrystalline chromium. J Less-Common Met. **27** 87–94 (1972). doi.org/10.1016/0022-5088(72)90108-7.

38. G. Simmons, Single Crystal Elastic Constants and Calculated Aggregate Progress,(1965).scholar.smu.edu/cgi/viewcontent.cgi?article=1029&context=journal_grc

39. P. Van Uffelen, C. Győri, A. Schubert et al., Extending the application range of a fuel performance code from normal operating to design basis accident conditions. J Nucl Mater. **383**, 137–143 (2008). doi.org/10.1016/j.jnucmat.2008.08.043

40.H.E. Rosinger, H.J. Neitzel, F.J. Erbacher, Development of a burst criterion for zircaloy fuel cladding under LOCA conditions. Res Mech. **2**, 91–107 (1981).

41. W.G. Luscher, K.J. Geelhood, Material Property Correlations: Comparisons between FRAPCON-3.4, FRAPTRAN 1.4, and MATPRO, Richland, WA (United States), (2010). doi.org/10.2172/1030897

42.J.L.Lamon,Properties and characteristics of sic and sic/sic composites,

Elsevier Inc. **2**, 323 (2012). doi:10.1016/B978-0-08-056033-5.00022-7

43. S. Liu, R. Liu, C. Qiu, CAMPUS-ANNULAR: Preliminary multiphysics modeling of annular fuel performance under normal operating and accident conditions, Prog Nucl Energy. **153**, 104430 (2022). doi.org/10.1016/j.pnucene.2022.104430

44. C.L. Wilson, C.L. Mohr, G.M. Hesson et al., LOCA Simulation in NRU Program - Data Report for the Fourth Materials Experiment (MT-4), (1983). doi.org/10.2172/5870315